Title

Tumor Radiosensitization by Monomethyl Auristatin E: Mechanism of Action and Targeted Delivery



Journal

Cancer Research, 75(7)

ISSN

0008-5472

Authors

Buckel, Lisa

Savariar, Elamprakash N

Crisp, Jessica L

et al.

Publication Date

2015-04-01

DOI

10.1158/0008-5472.can-14-1931

Peer reviewed

HHS Public Access

Author manuscript

*Cancer Res*. Author manuscript; available in PMC 2016 April 01.

Published in final edited form as:

*Cancer Res*. 2015 April 1; 75(7): 1376–1387. doi:10.1158/0008-5472.CAN-14-1931.

# Tumor radiosensitization by monomethyl auristatin E: mechanism of action and targeted delivery

**Lisa Buckel**[#1], **Elamprakash N. Savariar**[#2], **Jessica L. Crisp**[2], **Karra A. Jones**[3], **Angel M. Hicks**[1], **Daniel J. Scanderbeg**[1], **Quyen T. Nguyen**[4], **Jason K. Sicklick**[5], **Andrew M. Lowy**[5], **Roger Y. Tsien**[2,6], and **Sunil J. Advani**[1,7,*]

[1]Department of Radiation Medicine and Applied Sciences

[2]Department of Pharmacology

[3]Department of Pathology Department of Surgery

[4]Division of Head and Neck Surgery

[5]Division of Surgical Oncology

[6]Howard Hughes Medical Institute

[7]Center for Advanced Radiotherapy Technologies University of California San Diego

[#] These authors contributed equally to this work.

## Abstract

Intrinsic tumor resistance to radiotherapy limits the efficacy of ionizing radiation (IR). Sensitizing cancer cells specifically to IR would improve tumor control and decrease normal tissue toxicity. The development of tumor targeting technologies allows for developing potent radiosensitizing drugs. We hypothesized that the anti-tubulin agent monomethyl auristatin E (MMAE), a component of a clinically approved antibody-directed conjugate, could function as a potent radiosensitizer and be selectively delivered to tumors using an activatable cell penetrating peptide targeting matrix metalloproteinases and RGD binding integrins (ACPP-cRGD-MMAE). We evaluated the ability of MMAE to radiosensitize both established cancer cells and a low passage cultured human pancreatic tumor cell line using clonogenic and DNA damage assays. MMAE sensitized colorectal and pancreatic cancer cells to IR in a schedule and dose dependent manner correlating with mitotic arrest. Radiosensitization was evidenced by decreased clonogenic survival and increased DNA double strand breaks in irradiated cells treated with MMAE. MMAE in combination with IR resulted in increased DNA damage signaling and activation of CHK1. To test a therapeutic strategy of MMAE and IR, PANC-1 or HCT-116 murine tumor xenografts were treated with non-targeted free MMAE or tumor targeted MMAE (ACPP-cRGD-MMAE). While free MMAE in combination with IR resulted in tumor growth delay, tumor targeted ACPP-cRGD-MMAE with IR produced a more robust and significantly prolonged tumor regression in xenograft models. Our studies identify MMAE as a potent radiosensitizer. Importantly, MMAE radiosensitization can be localized to tumors by targeted activatable cell penetrating peptides.

[*]Corresponding Author Sunil J. Advani Department of Radiation Medicine and Applied Sciences Moores Cancer Center University of California San Diego 3855 Health Sciences Drive, MC 0843 La Jolla, CA 92093-0843 Phone: 858-822-6046 Fax: 858-822-5568 sjadvani@ucsd.edu.

## Introduction

Locally advanced tumors are commonly treated with combination chemotherapy and radiotherapy. In randomized clinical trials, concurrent chemotherapy-radiotherapy has demonstrated improved local tumor control and overall survival, including gastrointestinal tumors (1-4). A principal rationale for using concurrent chemotherapy with radiotherapy is the ability of chemotherapy drugs to radiosensitize. Radiosensitizers increase ionizing radiation (IR) mediated DNA damage and tumor cell kill (5-7). To be clinically useful, radiation sensitizers must improve the therapeutic index, i.e. the level of sensitization of tumor cells must be greater than that of normal tissue. A major limitation to using more potent radiosensitizers is the inability to deliver such agents specifically to the tumor.

Cell sensitivity to IR varies throughout the cell cycle with $G_2$/M being the most sensitive phase (8). Chemotherapy drugs such as paclitaxel block cells in $G_2$/M, function as radiosensitizers, and are used clinically with radiotherapy (9). Monomethyl auristatin E (MMAE) is a synthetic derivative of dolastatin 10 and functions as a potent anti-mitotic agent by inhibiting tubulin polymerization (10). We therefore tested the ability of MMAE to function as a radiosensitizer. However like many potent anti-tumor agents, systemic delivery of MMAE is limited by toxicity. When MMAE delivery is tumor restricted by conjugation to a CD30 targeting antibody (brentuximab vedotin), its efficacy becomes clinically apparent for lymphomas (11-12).

To evaluate the ability of targeted MMAE tumor delivery to radiosensitize tumors we used activatable cell penetrating peptide (ACPP) technology. ACPP can function as tumor targeted delivery vehicles (13-16). MMAE has recently been conjugated to ACPP-cRGD as a therapeutic payload (ACPP-cRGD-MMAE) in murine models of breast cancer (17). ACPPs consist of four regions: a polyanionic autoinhibitory domain, a protease sensitive peptide linker region, a cell penetrating polycationic peptide, and the payload to be delivered. The polycationic cell penetrating peptide consists of nine D-arginines ($r_9$), and the autoinhibitory portion is nine D-glutamates ($e_9$). A flexible peptide linker separates these two domains. For therapeutic applications, anti-cancer drugs are the payload conjugated to the polycationic cell penetrating peptide portion to facilitate their intracellular delivery (17). While the ACPP is intact, the polyanion region prevents adhesion and uptake of the polycationic cell penetrating peptide plus payload. Upon extracellular protease attack on the linker region, drug conjugated-$r_9$ is released and taken up by cells, where a second protease in the endocytic pathway releases the drug from the $r_9$. Tumor specific activation of ACPP has been achieved by inserting a PLGC(Me)AG linker sequence between the polyanionic and polycationic regions. Cleavage of this peptide linker is dependent on gelatinases, matrix metalloproteinases (MMP) 2 and 9. To augment MMP activity and cleavage of PLGC(Me)AG, the ACPP was designed to co-target RGD binding integrins. $\alpha_v\beta_3$ integrin binds to the hemopexin domain of MMP-2 and enhances MMP activation (18).

Here we evaluated the ability of MMAE to radiosensitize tumor cells and to be targeted to tumor xenografts in combination with IR. We show MMAE arrests cells in $G_2$/M in the 1-5 nM range and has an $IC_{50}$ that is > 6 fold lower than paclitaxel. Of significance, we

demonstrate that in addition to its intrinsic anti-tumor activity, MMAE sensitized cells to IR. MMAE radiosensitization showed both schedule and dose dependency, with MMAE radiosensitization directly correlating with accumulation of cells in $G_2$/M. In irradiated cells treated with MMAE, there was decreased clonogenic survival and increased activation of the DNA damage response. We then evaluated a therapeutic strategy of combining MMAE with IR in murine tumor xenograft models. We tested both non-targeted and tumor targeted MMAE delivery in PANC-1 and HCT-116 xenografts. For tumor targeted delivery, we utilized ACPP-cRGD-MMAE. Combining ACPP-cRGD-MMAE with IR in either HCT-116 or PANC-1 tumor xenografts resulted in prolonged tumor xenograft regression that was not observed with IR or ACPP-cRGD-MMAE alone. Moreover, the advantage of tumor targeted MMAE delivery was demonstrated in irradiated tumor xenografts. ACPP-cRGD-MMAE tumor targeted delivery increased tumor xenograft control compared to free MMAE. Our results lay the foundation to test a therapeutic treatment paradigm in which selective and potent radiosensitization can be achieved with tumor targeted ACPP.

## Materials and Methods

### Cells and Reagents

Human colorectal HCT-116 (ATCC CCL-247), pancreatic PANC-1 (ATCC CRL-1469) adenocarcinoma cell lines were directly obtained from American Type Culture Collection (STR tested) and passaged for less than 6 months following resuscitation. 779E is a limited passage pancreatic adenocarcinoma cell line developed in the Lowy laboratory from patient derived pancreatic adenocarcinoma xenograft. 779E has been whole exome sequenced in 2014 for mutational status and also was confirmed to be human origin. The XPA-1 cell line was initially derived from a patient derived pancreatic xenograft from Johns Hopkins and provided by the Lowy laboratory. Cells were negative for mycoplasma prior to use in experiments. Cells were cultured in DMEM supplemented with 10% FBS. For patient derived pancreatic adenocarcinoma xenografts (PDX), primary tumors from patients were directly implanted orthotopically into NOD SCID gamma (NSG) mice and passaged serially by orthotopic re-implantation. Paclitaxel (Sigma) and MMAE (Concortis) were both reconstituted in DMSO. ACPP and ratiometric ACPP peptides were synthesized as previously reported (17, 19).

### Cell cycle and Apoptosis

Cells were treated with MMAE for 24 hours and then fixed in methanol. Cells were treated with RNAse, stained with propidium iodide (PI) and analyzed by FACS using FloJo software.

### Alamar Blue assay

Cells were plated in 96 well plates and exposed to MMAE or paclitaxel for 72 hours and analyzed at 560 nm. For irradiated cells, cells were treated with MMAE overnight followed by 6 Gy.

### Clonogenic assay

Cells were treated with MMAE for 24 hours and then irradiated with 0-8 Gy. Following IR, cells were re-plated in drug free media. Colonies formed over 10-14 days and were counted.

### Neutral comet assay

Cells were treated for indicated length and doses of MMAE followed by 6 Gy. Cells were harvested 15 minutes post IR, underwent neutral electrophoresis (Trevigen). Comet tails were counted in multiple fields (>60 cells per sample) and analyzed using CometScore (TriTek Corp).

### γH2Ax immunostaining

Cells grown on glass cover slips were treated with MMAE overnight and then irradiated. Two hours post IR, cells were fixed, permeabilized and stained with antibody to γH2Ax. Nuclei were stained with DAPI. Foci were counted in 6-8 high power fields per group.

### Immunoblotting

MMAE and IR treated cells were harvested and lysed in RIPA buffer with protease and phosphatase inhibitors (Roche). 30 ug of lysate underwent electrophoresis using 4-12% Bis-Tris gels (Life Technologies), transferred to PVDF membranes and incubated with indicated primary antibodies (Cell Signaling Technology). Blots were developed by ECL (Pierce).

### Tumor xenograft gel zymography

All animal work was done in compliance with the UCSD Institutional Animal Use and Care Committee. 6-8 week old female athymic nu/nu mice (UCSD Animal Care Program) were injected subcutaneously into thighs with $5\times10^6$ HCT-116 or PANC-1 cells in a 1:1 Matrigel (BD) and PBS solution. After tumors grew to >200 $mm^3$, the right tumor hindlimb was focally irradiated while the remainder of the mouse including the left tumor hindlimb were shielded from IR with custom lead blocking > 95% of the dose as verified by dosimeters placed on the mouse. Tumors were excised from animals one day post IR. Non-irradiated pancreatic adenocarcinoma PDX tumors were also tested for gelatinase activity. Tris-SDS buffer was added at a ratio of 9 μL buffer per mg of tissue. Tumors were homogenized, centrifuged, and the supernatant diluted 1:1 with PBS. 2X Tris-glycine sample buffer was added and the samples were run on zymography gels (Life Technologies). The gels were placed in renaturing buffer, then transferred to developing buffer (Life Technologies).

### Immunohistochemistry

Mice were treated with IR or intravenous (IV) injection of ACPP-cRGD-MMAE, tumor tissue was harvested, formalin fixed and paraffin embedded followed by staining with indicated antibodies (Ventana Medical Systems). The primary antibody was used at a 1:250 dilution and was visualized using DAB as a chromagen with the UltraMap system (Ventana Medical Systems).

### In vivo tumor xenograft optical imaging

Tumor xenografts were irradiated as described above. One day post IR, mice were anesthetized (1:1 mixture of 100 mg/ml of ketamine and 5 mg/ml of midazolam) and IV injected with either fluorescently labeled ratiometric ACPP (Cy5 and Cy7) or ACPP-cRGD-MMAE (Cy5). Animals were imaged 2 hours later using a Maestro Small Animal Imager (CRI) with excitation filter of 620/22 nm and 645 nm long pass emission filter with dichroic filter tuned to 670 nm. Imaging was done both with skin on and after skin removal to decrease autofluorescence and scattering.

### In vivo tumor xenograft experiments

HCT-116 or PANC-1 tumor growth was measured with digital calipers. Tumor volume was calculated using the formula as ½ * Length * Width$^2$. Mice were randomized into groups as indicated in **Results** once the average tumor volume reached >200 mm$^3$. Free MMAE was injected on an equimolar basis to ACPP-cRGD-MMAE.

### Statistical Analysis

Unpaired 2-sided t tests were performed for $IC_{50}$ and radiosensitization experiments in cell culture. In tumor regression studies, 2-way ANOVA analysis was performed with Tukey's multiple comparison group. All statistical analyses were performed using Prism software (GraphPad)

## Results

### Cytotoxicity of MMAE against tumor cell lines

We first tested the ability of MMAE to block proliferating tumor cells in $G_2$/M. Established tumor cell lines (HCT-116 and PANC-1) were exposed to MMAE for 24 hrs and then collected. HCT-116 and PANC-1 cells showed a dose response accumulation of cells in the $G_2$/M, with PANC-1 cells more sensitive to MMAE than HCT-116 cells (**Fig. 1A**). 5 nM MMAE resulted in 50% of HCT-116 cells blocked in $G_2$/M and 2 nM in PANC-1 cells.

We next compared the cytotoxicity of MMAE to paclitaxel. Tumor cells were exposed to MMAE or paclitaxel for 72 hours and cell viability was assessed. For HCT-116, the $IC_{50}$ for paclitaxel and MMAE were 10.0 nM and 1.7 nM (**Fig. 1B, D**). For PANC-1, the $IC_{50}$ for paclitaxel and MMAE were 15.1 nM and 0.6 nM (**Fig. 1C, D**). We also tested a limited passage human pancreatic tumor cell line, 779E. 779E was more resistant to both anti-mitotic agents, however it also showed increased sensitivity to MMAE. The $IC_{50}$ following paclitaxel or MMAE exposure were 52.0 nM and 5.6 nM respectively (**Fig. 1D**).

### Interaction of MMAE and IR to increase DNA double strand breaks

Since MMAE blocks cells in the radiosensitive $G_2$/M phase of the cell cycle, we tested if MMAE specifically interacted with IR. We hypothesized that while a short exposure to MMAE would not influence radiosensitivity, prolonged MMAE exposure with cells accumulating in $G_2$/M would increase sensitivity to IR. DNA double stand breaks are a hallmark of IR damage and can be measured by neutral comet assay. HCT-116 cells were treated with 5 nM MMAE for varying lengths of time (0, 2, 4, or 24 hrs) and then irradiated

(**Fig. 2A**). Irradiation of cell exposed to MMAE for 2 or 4 hr did not increase comet tail length compared to IR alone. However 24 hr exposure to MMAE significantly increased comet tail length in irradiated cells compared to vehicle or shorter MMAE exposure time. Immunoblotting for cell phase specific cyclins demonstrated that 24 hour MMAE exposure resulted in the specific accumulation of the $G_2$/M cyclin B compared to non-mitotic cyclins. A similar schedule dependence of MMAE on IR induced DNA damage was observed in PANC-1 cells (**Supplemental Fig. 1A**).

Next we evaluated if 24 hour exposure to MMAE increased IR induced DNA breaks in a dose dependent manner. In irradiated HCT-116 cells, treating with 1 nM MMAE did not increase DNA damage over IR alone. However, 5 nM MMAE resulted in a significant increase in IR induced DNA double-stranded breaks. These results are concordant with dose response effects of MMAE on cell cycle in HCT-116 cells, where 1 nM of MMAE did not alter the cell cycle profile but 5 nM did (**Fig. 1A**). Overnight MMAE exposure also significantly increased comet tail length following IR in XPA-1 and 779E cells (**Supplemental Fig. 1B, C**).

## MMAE decreases clonogenic survival in irradiated cells

Since MMAE increased IR induced DNA double strand breaks, we determined if MMAE decreased survival in irradiated cells. In the first series of experiments, HCT-116 and PANC-1 tumor cell lines were incubated with varying doses of MMAE overnight and then irradiated with 6 Gy the following day. Cells were continuously exposed to MMAE, and tumor cell viability was measured 72 hours after initiation of MMAE treatment. In HCT116 cells, the $IC_{50}$ for MMAE decreased from 1.6 nM for MMAE alone treated cells to 0.8 nM in cells treated with MMAE and IR (**Fig. 3A**). In PANC-1 cells, a similar relative reduction (≈50%) in the $IC_{50}$ of MMAE was observed. In non-irradiated PANC-1 cells the $IC_{50}$ for MMAE was 0.8 nM, which decreased to 0.4 nM when IR was combined with MMAE (**Fig. 3B**).

The primary mode of cell death following IR is mitotic catastrophe. Therefore, we tested the ability of MMAE to decrease clonogenic cell survival. HCT-116 or PANC-1 cells were exposed to MMAE overnight and then irradiated with 0-8 Gy. Based on the cell cycle dose response to MMAE from **Fig 1A**, we treated HCT-116 cells with 5 nM and PANC-1 cells with 2 nM of MMAE. Following irradiation, cells were re-plated in drug free media at low cell density and colonies grew out over 10-14 days. Cell surviving fractions were normalized to 1 for non-irradiated cells treated with either vehicle or MMAE. MMAE resulted in increased tumor cell kill at doses as low as 2 Gy (**Fig. 3C, D**). Since conventionally fractionated radiotherapy for tumors is often given with 2 Gy concurrently with chemotherapy, we measured the surviving fraction at 2 Gy (SF2) with varying doses of MMAE. For HCT116, the SF2 for cells treated with 1 nM MMAE was not significantly different from vehicle treated cells. However, at doses of 2 and 5 nM MMAE there was a significant reduction in the SF2 compared to cells irradiated with vehicle (**Fig. 3E**). Consistent with our above results with MMAE alone, irradiated PANC-1 cells showed increased sensitivity at lower MMAE doses. The SF2 in PANC-1 cells was significantly reduced with 1 or 2 nM of MMAE compared to vehicle treated cells, (**Fig. 3F**).

### MMAE increases DNA damage response in irradiated cells

Since MMAE reduced clonogenic cell survival following IR, we tested if MMAE increased apoptosis in irradiated cells. HCT-116 cells were treated with MMAE for 24 hrs followed by IR. Cells were collected 24 hrs post IR and the sub G1 population (apoptotic) was measured. MMAE alone resulted in a significant increase in apoptosis compared vehicle treated cells (**Fig 4A**). However, there was no further increase in apoptosis when IR was combined with MMAE. Since MMAE increased DNA double strand breaks in irradiated cells (**Fig. 2**), we then evaluated if MMAE altered the DNA damage response in irradiated cells. HCT-116 cells were treated with MMAE for 24 hrs followed by 6 Gy. Cells were collected 1 hour post IR and activation of the DNA damage checkpoint proteins CHK1 (pS345) and CHK2 (pT68) was ascertained (**Fig. 4B**). Interestingly, MMAE enhanced CHK1 activation in irradiated cells, while CHK2 activation was not affected. Upon DNA damage, H2A becomes phosphorylated at S139, γH2AX. MMAE significantly increased γH2AX foci formation in irradiated HCT-116 and PANC-1 cells (**Fig. 4C, D, Supplemental Fig. 2**). In non-irradiated cells, MMAE did not alter DNA damage.

### Pancreatic and colorectal tumor xenografts express protease activity against PLGC(Me)AG-ACPP peptide linker

While MMAE is a potent cytotoxic molecule in cell culture and an effective radiosensitizer, normal tissue toxicity is a limiting factor to exploit it therapeutically *in vivo*. To target MMAE to tumors, we used MMAE conjugated to a dual integrin and MMP targeted ACPP, ACPP-cRGD-MMAE (17). The linker region of this ACPP is a substrate for MMP-2 and MMP-9. We first tested if orthotopically grown patient derived pancreatic adenocarcinoma xenografts (PDX) expressed MMP activity. Two unique PDX xenografts both contained gelatinase activity (**Fig. 5A**). Next, we tested if HCT-116 and PANC-1 tumor xenografts had gelatinase activity. Non-irradiated HCT-116 and PANC-1 tumor lysates both contained gelatinase activity as measured by gel zymography (**Fig. 5B**). We also tested if tumor irradiation altered MMP activity. Tumor xenografts were irradiated with a single dose of 6 Gy and harvested the following day. Irradiation of tumors did not hamper gelatinase activity. Since ACPP-cRGD-MMAE is co-targeted to cRGD binding integrin $\alpha_v\beta_3$, we analyzed $\beta_3$ integrin expression and found that PANC-1 and HCT-116 tumors expressed $\beta_3$ integrin (**Fig. 5C, Supplemental Fig. 3**). One day post IR, irradiated tumors also abundantly expressed $\beta_3$ integrin.

To directly assess if HCT-116 and PANC-1 tumor xenografts can cleave the PLGC(Me)AG linker region incorporated into ACPP-cRGD-MMAE, we utilized a ratiometric ACPP probe with the same MMP substrate sequence (19). Ratiometric ACPP has a Cy5 far red fluorescent donor and Cy7 near infrared fluorescent acceptor. While intact, the peptide will favor Cy7 re-emission when excited with Cy5 excitation wavelengths, resulting in a low Cy5:Cy7 emission ratio (blue pseudocolor). However, when the peptide is cleaved, Cy5 emission is no longer quenched resulting in a higher Cy5:Cy7 emission ratio (red pseudocolor). Tumors were grown in the bilateral hindlimbs. The right hindlimb tumor bearing region was irradiated while the left hindlimb tumor was shielded. The following day ratiometric ACPP (10 nmoles) was injected intravenously and mice were imaged 2 hours later. Tumors were imaged in situ and after excision. In both HCT-116 and PANC-1 tumors,

tumors had increase in Cy5:Cy7 emission ratio compared to surrounding normal tissue, which is indicative of tumor protease activity cleaving the linker region within the ACPP molecule and releasing the polycationic cell penetrating peptide (**Fig. 5D, Supplemental Fig. 4A**). Irradiation of tumors one day prior to ratiometric ACPP injection did not diminish peptide cleavage compared to non-irradiated tumors. Interestingly, there was a trend towards increased Cy5:Cy7 emission ratio in irradiated tumors compared to non-irradiated tumors (**Supplemental Fig. 4B**).

## Therapeutic efficacy of combining an integrin and MMP targeted ACPP-cRGD-MMAE with ionizing radiation

We next tested a therapeutic paradigm of using of ACPP-cRGD to deliver the potent radiosensitizer, MMAE. We first validated that MMAE conjugated to the polycationic cell penetrating peptide ($r_9$) was cytotoxic to tumor cells. HCT-116, PANC-1 and 779E cells were exposed to $r_9$ alone or $r_9$ conjugated to MMAE ($r_9$-MMAE). Carrier $r_9$ alone had no cytotoxicity, whereas $r_9$-MMAE produced cytotoxicity in all three tumor cell lines (**Supplemental Fig. 5**). We then tested if ACPP-cRGD-MMAE accumulated in HCT-116 and PANC-1 tumor xenografts. ACPP-cRGD-MMAE with a Cy5 dye attached to the polycation region was intravenously injected. Tumors were imaged 6 hours later. As with ratiometric ACPP (**Fig. 5D**), ACPP-cRGD-MMAE accumulated in both the non-irradiated and irradiated tumor xenografts (**Fig. 6A**). To determine if ACPP-cRGD-MMAE delivered functionally active MMAE within the tumor, HCT-116 tumor xenografts were harvested 24 hrs following ACPP-cRGD-MMAE IV injection and stained for the mitotic marker, pS10 Histone H3 (**Fig. 6B**). In mice IV injected with ACPP-cRGD-MMAE, tumor xenografts demonstrated a 32% increase in pS10 Histone H3 staining compared to vehicle treatment, $p=0.002$.

We then evaluated the efficacy of combined MMAE with focal IR to inhibit tumor xenograft growth. First, we tested the hypothesis that MMAE tumor targeted delivery would increase tumor regression compared to free MMAE delivery (**Fig. 6C)**. PANC-1 tumor xenografts were grown to a mean volume of 200 $mm^3$ prior to initiation of therapy. Free MMAE or ACPP-cRGD-MMAE was IV injected on days 0 and 1 (6 nmoles of MMAE/day). This dose of MMAE was chosen based on prior studies on animal toxicity associated with free MMAE delivery. Fractionated IR of 3 Gy per day was given on day 1 and 2. On day 1 when MMAE and IR were both given, IR was delivered in the morning and MMAE in the afternoon. By day 30 following initiation of therapy, free MMAE treatment resulted in a small but statistically significant growth delay of PANC-1 tumors compared to untreated control tumors, $p<0.0001$. The average tumor volume of free MMAE treated mice was 75% of untreated controls. More importantly, free MMAE in combination with IR resulted in profound tumor xenograft regression compared to IR or free MMAE alone ($p<0.0001$). In comparing targeted and free MMAE delivery in the absence of IR, ACPP-cRGD-MMAE resulted in significantly greater tumor regression compared free MMAE, which is consistent with prior studies involving breast cancer models (12). Of significance, IR combined with ACPP-cRGD-MMAE resulted in prolonged tumor regression when compared to free MMAE and IR ($p<0.01$). Longer follow up of tumors demonstrated that 2 of 10 PANC-1 tumors treated with ACPP-cRGD-MMAE and IR were less than or equal to their starting

tumor volume on day 0 (**Table 1**). Of significance, such prolonged and sustained tumor regression was observed with only 2 doses of both MMAE and IR and the initial tumor volume was greater than 200 $mm^3$. Moreover, no other treatment group showed long term tumor regression.

We extended our studies on ACPP-cRGD-MMAE and IR by increasing the dosing schedule to see if it would result in further improvement in long term regression. ACPP-cRGD-MMAE was given on days 0, 1, and 2 (6 nmoles/day, 18 nmoles total). Fractionated IR of 3 Gy per day was administered on day 1, 2, and 3. Again on days when ACPP-cRGD-MMAE and IR were both given, IR was delivered in the morning and ACPP-cRGD-MMAE in the afternoon. As we observed in **Fig 6C**, combining ACPP-cRGD-MMAE with IR again produced significant tumor regression compared to IR or ACPP-cRGD-MMAE alone treated mice (**Supplemental Fig. 6**). Tumor volumes in the combined ACPP-cRGD-MMAE and IR mice remained statistically significant compared to all other groups, $p<0.0001$. More striking and of therapeutic importance, the majority of treated tumors had prolonged tumor regression in PANC-1 tumors upon combining ACPP-cRGD-MMAE with IR. By day 40, none of the control or IR alone treated tumors were smaller than their initial tumor volume on day 0 (**Table 1**). For the ACPP-cRGD-MMAE alone group, only 1 of 14 tumors was smaller than their initial tumor volumes. In contrast, 8 of 14 tumors in the combined ACPP-cRGD-MMAE and IR group were smaller than their initial tumor volume.

We then tested a modified treatment schedule of ACPP-cRGD-MMAE and IR using HCT-116 tumor xenografts. HCT-116 tumors were grown to mean tumor volume of > 270 $mm^3$ prior to initiation of therapy. We had observed that 6 Gy given to HCT-116 xenografts improved ratiometric ACPP probe cleavage (**Fig. 5D** and **Supplemental Fig. 4**). Therefore in irradiated tumors, we delivered 6 Gy on day 0 followed by 3 Gy on days 1 and 2. ACPP-cRGD-MMAE was IV injected on days 0 and 1, six hours following irradiation (7.5 nmoles/day). The dose of ACPP-cRGD-MMAE was increased compared to PANC-1 since HCT-116 cells had a higher $IC_{50}$ for MMAE. As seen in PANC-1 tumors, ACPP-cRGD-MMAE alone produced a modest growth delay compared to untreated control tumors (**Fig. 6D**). As expected, IR alone resulted in an initial tumor growth delay (especially prominent due to the 6 Gy dose on day 0), however by day 10, tumor volume began to rise. Combining ACPP-cRGD-MMAE with IR again produced sustained tumor regression compared to IR alone starting at day 10 post initiation of therapy, $p<0.006$. By day 14, none of the control or ACPP-RGD-MMAE treated tumors were smaller than their initial tumor volume on day 0 (**Table 1**). For the IR alone group, only 3 of 10 tumors were smaller than their initial tumor volume. In contrast, 9 of 10 tumors in the combined ACPP-cRGD-MMAE and IR group were smaller than their initial tumor volume.

## Discussion

In these series of studies we have identified that MMAE can radiosensitize tumor cells and enhance tumor xenograft regression in combination with IR. Moreover, we tested a therapeutic paradigm whereby a potent radiosensitizer such as MMAE can be selectively delivered to tumors using activatable cell penetrating peptides to increase tumor response to IR (**Supplemental Fig. 7**). MMAE, a synthetic derivative of dolastatin 10, sensitizes cancer

cells to IR mediated DNA damage and cell kill (10). Intrinsic tumor cell resistance to IR is dependent on a multitude of factors, including activity of DNA repair pathways, tumor oxygenation status and the cell cycle (5-7). By pharmacologically targeting these pathways, cells become more sensitive to the effects of IR. An optimal cancer therapeutic agent would have the dual benefit of single agent potent tumoricidal activity and also sensitize tumors to IR. Our data support MMAE as a candidate that meets such requirements.

MMAE has previously been shown to have single agent anti-tumor efficacy against a broad panel of tumor histologies when appropriately delivered (17, 20, 21). In our own studies with established cancer cells and a limited patient passage patient derived pancreatic adenocarcinoma cell line, MMAE had an $IC_{50}$ that is at least 6 fold lower than paclitaxel (**Fig. 1**). MMAE is an anti-tubulin agent that blocks cells in $G_2$/M, and the $G_2$/M phase of the cell cycle is the most sensitive to the IR (8). We demonstrated that MMAE increased IR induced DNA double strand breaks in both a schedule and dose dependent manner that directly correlated with the accumulation of cells in $G_2$/M (**Fig 1, 2**). MMAE also decreased clonogenic survival of pancreatic and colorectal cancer cells in the 1-5 nM range in combination with IR indicative of its application as a potent radiosensitizer. Mechanistically, MMAE increased clonogenic cell death in irradiated cells. The decreased cell survival following combined IR and MMAE was not due to apoptosis, suggesting mitotic catastrophe as the cause of MMAE enhanced cell death in irradiated cells. In support of this, MMAE enhanced the DNA damage response pathway in irradiated cells. Both γH2AX foci formation and activation of CHK1 were increased in cells treated with MMAE prior to irradiation. Understanding the cellular response to MMAE can allow for future rational drug combinations with MMAE to further augment radiosensitization by inhibiting survival pathways induced by MMAE.

While MMAE is a potent radiosensitizer *in vitro*, it requires tumor targeted delivery to achieve a clinically meaningful therapeutic index in *vivo*. We have therefore initially evaluated a strategy using MMP and cRGD binding integrin targeted ACPP delivery of MMAE in combination with focal IR (17). A major limitation to the therapeutic utility of radiosensitizers is the lack of tumor specific delivery (22, 23). Radiosensitizer delivery that is non-targeted can result in increased radiosensitization of not only tumor cells, but also surrounding normal tissue. This results in no net gain in the therapeutic index of radiotherapy. Previous reports have tested nanoparticles as radiosensitizer delivery vehicles (24-27). Here, we have demonstrated the efficacy of ACPP technology to deliver the potent radiosensitizer MMAE specifically to tumors. Following MMP-2/9 and $\alpha_v\beta_3$ integrin targeted delivery and release of MMAE conjugated cell penetrating peptide from the ACPP, tumor xenografts demonstrated prolonged regression in combination with IR compared to non-targeted free MMAE delivery (**Fig. 6, Table 1**). Moreover at equimolar systemic IV injection, ACPP-cRGD-MMAE improved tumor xenograft regression when compared to non-targeted MMAE for both non-irradiated and irradiated tumors. We also tested altering the order of delivery of IR and ACPP-cRGD-MMAE. In the PANC-1 xenograft experiments, ACPP-cRGD-MMAE was initially injected one day prior to 3 Gy fractions of IR (**Fig. 6 and Supplemental Fig. 6**). These experiments were designed based on MMAE functioning as a radiosensitizer by blocking tumor cells in $G_2$/M. Therefore, MMAE was

injected into mice prior to irradiation. To test the ability of IR to modulate the tumor environment and increase ACPP-cRGD-MMAE tumor accumulation, we altered the treatment scheduling, with a larger 6 Gy dose given 1 day prior to ACPP-cRGD-MMAE injection in HCT-116 xenografts (**Fig. 6D**). The rationale for an initial 6 Gy in HCT-116 tumor xenograft experiment was twofold. First, HCT-116 tumors grow more rapidly in our tumor model compared to PANC-1 tumor xenografts. Secondly, a dose of 6 Gy increased ratiometric ACPP activation in irradiated tumors compared to non-irradiated tumors (**Fig. 5D and Supplemental Fig. 4)**. Therefore, we hypothesized that pre-irradiation would increase ACPP mediated delivery of MMAE to irradiated tumor xenografts. Following the initial 6 Gy dose to increase ACPP mediated MMAE delivery, 2 doses of 3 Gy were given post ACPP-cRGD-MMAE. Even with a total dose delivered of 12 Gy to HCT-116 tumors over 3 days, the majority of HCT-116 tumors began to regrow in contrast to combined treatment with ACPP-cRGD-MMAE. While the treatment regimens in the three xenograft experiments varied from each other, a strength is that their conclusions consistently demonstrated that combining ACPP-cRGD-MMAE with IR resulted in sustained tumor xenograft regression (**Table 1**).

ACPP conjugated delivery of radiosensitizers is innovative and of clinical significance in that it offers a solution to the problem of non-selective radiosensitization of molecules for not only cancer cells but also surrounding normal tissue. In addition, it provides a mechanism for efficient intracellular delivery and release of the conjugated drug payload, i.e. MMAE. MMAE is conjugated to the polycationic cell penetrating peptide portion of ACPP through a cathepsin B sensitive linker (valine-citrulline) (17). Once the ACPP peptide linker is cleaved in the tumor microenvironment, the cell penetrating peptide-MMAE is internalized and free MMAE released from lysosomes through the action of cathepsin B. Such a therapeutic paradigm can allow for the clinical development and testing of more potent radiosensitizers since systemic toxicity and collateral normal tissue damage would be decreased. Since MMP activity is high in the tumor microenvironment, MMP-2/9 targeted ACPP may also be a broadly applicable tumor selective delivery vehicle for radiosensitizers. Meanwhile, the only immediately clinically approved vehicle for MMAE delivery is brentuximab vedotin, with a host of similar antibody-MMAE conjugates undergoing clinical trial (11, 28). Our results showing radiosensitization by free MMAE in vitro suggest that antibody-MMAE conjugates should show similar radiosensitization, since the antibody is another mechanistic targeting vector for MMAE. Viewed another way, IR may be a valuable adjunct to chemotherapy with antibody-drug conjugates.

Our work also lays the foundation for further refinement of radiation guided ACPP delivery of potent tumoricidal and radiosensitizing agents. IR results in changes in the tumor microenvironment including alterations of tumor permeability and retention, gene expression, tumor cell surface receptor expression and protease activity. The physics of IR allows for IR to be specifically deposited to tumor tissue and can allow it to serve as beaconing mechanism for systemically delivered therapeutic agents. Such a concept has been seen with combining IR with oncolytic viruses, where IR enhances the ability of both intratumoral and systemically delivered oncolytic viruses to replicate in irradiated tumor microenvironment (29-32). IR has also been used to induce the expression of neo-antigens

within tumors that can function as receptors for peptide ligand targeted nanoparticles (33-36). Interestingly, MMP activity has been reported to be induced in irradiated tumors, including patient derived rectal cancers (37-40). Moreover, the cRGD binding integrin $\alpha_v\beta_3$ expression is also upregulated by IR and modulates cell response to IR (41-44). While gelatin zymography of excised tumor xenografts did not reveal an increase in gelatinase activity in irradiated tumors compared to their non-irradiated counterparts, ratiometric PLGC(Me)AG linker ACPP showed a trend toward increase Cy5:Cy7 emission ratio in irradiated tumor xenografts compared to non-irradiated tumor xenografts (**Fig. 5 and Supplemental Fig. 4).** Our ratiometric PLGC(Me)AG linker ACPP contains both Cy5 (polycationic side) and Cy7 (polyanionic side), and real time ratiometric monitoring of tumors in mice has demonstrated tumor specific cleavage of this ratiometric probe (19). While Cy5 has increased tissue attenuation than Cy7, in our experience the greater extinction coefficient, quantum yield, and chemical stability of Cy5 compared to Cy7 make up for the somewhat greater attenuation (45). In addition, we have not found a ratiometric FRET donor-acceptor pair in which the donor is Cy7 and the acceptor is ~100 nm longer in wavelength.

An alternative explanation for the enhanced accumulation of ACPP within irradiated tumors as opposed to non-irradiated tumors is the concept of enhanced permeability and retention (EPR) of systemically delivered macromolecular agents of ≥40 KDa (46-48). IR has been shown to decrease the tumor interstitial pressure, especially with delivery of doses > 10 Gy. By decreasing tumor interstitial pressure, IR can augment diffusion of macromolecular drugs into the tumor. However, the ACPP-cRGD-MMAE is only 6.9 KDa, so it may not be affected as much by EPR. Using ratiometric ACPP probes, further optimization of radiation dose-fraction schedule may improve cleavage and activation of ACPP through increased expression of cRGD binding integrins and MMP 2/9 activity or increased tumor EPR. (**Fig. 5 and Supplemental Fig. 4**). Moreover, a radiation activatable cell penetrating peptide could be engineered in which a flexible peptide linker region could be inserted that is cleaved by IR induced tumor protease activity. This would increase ACPP cleavage dependence upon IR induced microenvironment proteases (**Supplemental Fig. 7**). Our results provide a conceptual basis for IR controlled ACPP to be developed that could deliver potent radiosensitizers. In such a treatment paradigm, there would be preferential accumulation of the radiosensitizer with the irradiated tumor and reduced bioavailability of the radiosensitizer to normal tissue. Such technology is not limited to radiosensitizer delivery. IR could be used to induce a “proteolytic switch” in the irradiated tumor target microenvironment to facilitate localized delivery of systemically administered cytotoxic anti-tumor agents.

## Supplementary Material

Refer to Web version on PubMed Central for supplementary material.

## Acknowledgments

The authors thank Joseph Aguilera, Evangeline Mose, Dawn Jaquish, Randy French and Donald P. Pizzo for excellent technical assistance.

Grant Support

This work was supported by grants from the NIH/NCI grant CA155620 (to AML), the Howard Hughes Medical Institute (to RYT), the NIH/NCI grant 5R01CA158448 (to ENS and RYT), the DoD Breast Cancer Collaborative Innovators Award W81XWH-09-1-0699 (to JLC and RYT), the American Cancer Society IRG #70-002 (to SJA), University of California Cancer Research Coordinating Committee (to SJA), UCSD Academic Senate (to SJA).

## References

1. Werner J, Combs SE, Springfeld C, Hartwig W, Hackert T, Büchler MW. Advanced-stage pancreatic cancer: therapy options. Nat Rev Clin Oncol. 2013; 10:323–33. [PubMed: 23629472]
2. Gutt R, Liauw SL, Weichselbaum RR. The role of radiotherapy in locally advanced pancreatic carcinoma. Nat Rev Gastroenterol Hepatol. 2010; 7:437–47. [PubMed: 20628346]
3. Aklilu M, Eng C. The current landscape of locally advanced rectal cancer. Nat Rev Clin Oncol. 2011; 8:649–59. [PubMed: 21826084]
4. Pretz JL, Wo JY, Mamon HJ, Kachnic LA, Hong TS. Chemoradiation therapy: localized esophageal, gastric, and pancreatic cancer. Surg Oncol Clin N Am. 2013; 22:511–24. [PubMed: 23622077]
5. Moding EJ, Kastan MB, Kirsch DG. Strategies for optimizing the response of cancer and normal tissues to radiation. Nat Rev Drug Discov. 2013; 12:526–42. [PubMed: 23812271]
6. Liauw SL, Connell PP, Weichselbaum RR. New paradigms and future challenges in radiation oncology: an update of biological targets and technology. Sci Transl Med. 2013; 5:173sr2. [PubMed: 23427246]
7. Raleigh DR, Haas-Kogan DA. Molecular targets and mechanisms of radiosensitization using DNA damage response pathways. Future Oncol.; 2013; 9:219–23.
8. Terasima T, Tolmach LJ. Variations in several responses of HeLa cells to xirradiation during the division cycle. Biophys J. 1963; 3:11–33. [PubMed: 13980635]
9. Tishler RB, Schiff PB, Geard CR, Hall EJ. Taxol: a novel radiation sensitizer. Int J Radiat Oncol Biol Phys. 1992; 122:613–7. [PubMed: 1346533]
10. Bai R, Pettit GR, Hamel E. Dolastatin 10, a powerful cytostatic peptide derived from a marine animal. Inhibition of tubulin polymerization mediated through the vinca alkaloid binding domain. Biochem Pharmacol. 1990; 39:1941–49. [PubMed: 2353935]
11. Doronina SO, Toki BE, Torgov MY, Mendelsohn BA, Cerveny CG, Chace DF, et al. Development of potent monoclonal antibody auristatin conjugates for cancer therapy. Nat Biotechnol. 2003; 21:778–84. [PubMed: 12778055]
12. Sievers EL, Senter PD. Antibody-drug conjugates in cancer therapy. Annu Rev Med. 2013; 64:15–29. [PubMed: 23043493]
13. Jiang T, Olson ES, Nguyen QT, Roy M, Jennings PA, Tsien RY. Tumor imaging by means of proteolytic activation of cell-penetrating peptides. Proc Natl Acad Sci U S A. 2004; 101:17867–72. [PubMed: 15601762]
14. Aguilera TA, Olson ES, Timmers MM, Jiang T, Tsien RY. Systemic in vivo distribution of activatable cell penetrating peptides is superior to that of cell penetrating peptides. Integr Biol (Camb). 2009; 1:371–81. [PubMed: 20023744]
15. Olson EA, Aguilera TA, Jiang T, Ellies LG, Nguyen QT, Wong EH, et al. In vivo characterization of activatable cell penetrating peptides for targeting protease activity in cancer. Integr Biol (Camb). 2009; 1:382–93. [PubMed: 20023745]
16. Whitney M, Crisp JL, Olson ES, Aguilera TA, Gross LA, Ellies LG, et al. Parallel in vivo and in vitro selection using phage display identifies protease-dependent tumor-targeting peptides. J Biol Chem. 2010; 285:22532–41. [PubMed: 20460372]
17. Crisp JL, Savariar EN, Glasgow HL, Ellies LG, Whitney MA, Tsien RY. Synergistic targeting of integrin avb3 and matrix metalloprotienase-2 improves optical imaging of tumors and chemotherapeutic efficiency. Mol Cancer Therapeutics. 2014; 13:1514–25.
18. Deryugina EI, Ratnikov B, Monosov E, Postnova TI, DiScipio R, Smith JW, et al. MT1-MMP initiates activation of pro-MMP-2 and integrin alphavbeta3 promotes maturation of MMP-2 in breast carcinoma cells. Exp Cell Res. 2001; 263:209–23. [PubMed: 11161720]

19. Savariar EN, Felsen CN, Nashi N, Jiang T, Ellies LG, Steinbach P, et al. Real-time in vivo molecular detection of primary tumors and metastases with ratiometric activatable cell-penetrating peptides. Cancer Res. 2013; 73:855–64. [PubMed: 23188503]
20. Ma D, Hopf CE, Malewicz AD, Donovan GP, Senter PD, Goeckeler WF, et al. Potent antitumor activity of an auristatin-conjugated, fully human monoclonal antibody to prostate-specific membrane antigen. Clin Cancer Res. 2006; 12:2591–6. [PubMed: 16638870]
21. Breij EC, de Goeij BE, Verploegen S, Schuurhuis DH, Amirkhosravi A, Francis J, et al. An antibody-drug conjugate that targets tissue factor exhibits potent therapeutic activity against a broad range of solid tumors. Cancer Res. 2014; 74:1214–26. [PubMed: 24371232]
22. Liu FF, Okunieff P, Bernhard EJ, Stone HB, Yoo S, Coleman CN, et al. Lessons learned from radiation oncology trials. Clin Cancer Res. 2013; 19:6089–100. [PubMed: 24043463]
23. Lin SH, George TJ, Ben-Josef E, Bradley J, Choe KS, Edelman MJ, et al. Opportunities and challenges in the era of molecularly targeted agents and radiation therapy. J Natl Cancer Inst. 2013; 105:686–93. [PubMed: 23503600]
24. Miller SM, Wang AZ. Nanomedicine in chemoradiation. Ther Deliv. 2013; 4:239–50. [PubMed: 23343162]
25. Werner ME, Cummings ND, Sethi M, Wang EC, Sukumar R, Moore DT, et al. Preclinical evaluation of Genexol-PM, a nanoparticle formulation of paclitaxel, as a novel radiosensitizer for the treatment of non-small cell lung cancer. Int J Radiat Oncol Biol Phys. 2013; 86:463–8. [PubMed: 23708084]
26. Joh DY, Sun L, Stangl M, Al Zaki A, Murty S, Santoiemma PP, Davis JJ, et al. Selective targeting of brain tumors with gold nanoparticle-induced radiosensitization. PLoS One. 2013; 8:e62425. [PubMed: 23638079]
27. Wang Y, Mo L, Wei W, Shi X. Efficacy and safety of dendrimer nanoparticles with coexpression of tumor necrosis factor-α and herpes simplex virus thymidine kinase in gene radiotherapy of the human uveal melanoma OCM-1 cell line. Int J Nanomedicine. 2013; 8:3805–16. [PubMed: 24124368]
28. Mullard A. Maturing antibody-drug conjugate pipeline hits 30. Nat Rev Drug Discov. 2013; 12:329–32. [PubMed: 23629491]
29. Hallahan DE, Mauceri HJ, Seung LP, Dunphy EJ, Wayne JD, Hanna NN, et al. Spatial and temporal control of gene therapy using ionizing radiation. Nat Med. 1995; 1:786–91. [PubMed: 7585181]
30. Mezhir JJ, Advani SJ, Smith KD, Darga TE, Poon AP, Schmidt H, et al. Ionizing radiation activates late herpes simplex virus 1 promoters via the p38 pathway in tumors treated with oncolytic viruses. Cancer Res. 2005; 65:9479–84. [PubMed: 16230412]
31. Advani SJ, Markert JM, Sood RF, Samuel S, Gillespie GY, Shao MY, et al. Increased oncolytic efficacy for high-grade gliomas by optimal integration of ionizing radiation into the replicative cycle of HSV-1. Gene Ther. 2011; 18:1098–102. [PubMed: 21544094]
32. Advani SJ, Buckel L, Chen NG, Scanderbeg DJ, Geissinger U, Zhang Q, et al. Preferential replication of systemically delivered oncolytic vaccinia virus in focally irradiated glioma xenografts. Clin. Cancer Res. 2012; 18:2579–2590. [PubMed: 22379115]
33. Hallahan DE, Qu S, Geng L, Cmelak A, Chakravarthy A, Martin W, et al. Radiation-mediated control of drug delivery. Am J Clin Oncol. 2001; 24:473–80. [PubMed: 11586099]
34. Hallahan D, Geng L, Qu S, Scarfone C, Giorgio T, Donnelly E, et al. Integrin-mediated targeting of drug delivery to irradiated tumor blood vessels. Cancer Cell. 2003; 3:63–74. [PubMed: 12559176]
35. Hariri G, Yan H, Wang H, Han Z, Hallahan DE. Radiation-guided drug delivery to mouse models of lung cancer. Clin Cancer Res. 2010; 16:4968–77. [PubMed: 20802016]
36. Passarella RJ, Spratt DE, van der Ende AE, Phillips JG, Wu H, Sathiyakumar V, et al. Targeted nanoparticles that deliver a sustained, specific release of Paclitaxel to irradiated tumors. Cancer Res. 2010; 70:4550–9. [PubMed: 20484031]
37. Fujita M, Otsuka Y, Yamada S, Iwakawa M, Imai T. X-ray irradiation and Rho-kinase inhibitor additively induce invasiveness of the cells of the pancreatic cancer line, MIAPaCa-2, which exhibits mesenchymal and amoeboid motility. Cancer Sci. 2011; 102:792–8. [PubMed: 21214671]

38. Lee WH, Warrington JP, Sonntag WE, Lee YW. Irradiation alters MMP-2/TIMP-2 system and collagen type IV degradation in brain. Int J Radiat Oncol Biol Phys. 2012; 82:1559–66. [PubMed: 22429332]

39. Speake WJ, Dean RA, Kumar A, Morris TM, Scholefield JH, Watson SA. Radiation induced MMP expression from rectal cancer is short lived but contributes to in vitro invasion. Eur J Surg Oncol. 2005; 31:869–74. [PubMed: 16081236]

40. Kumar A, Collins HM, Scholefield JH, Watson SA. Increased type-IV collagenase (MMP-2 and MMP-9) activity following preoperative radiotherapy in rectal cancer. Br J Cancer. 2000; 82:960–5. [PubMed: 10732772]

41. Xu W, Luo T, Li P, Zhou C, Cui D, Pang B, et al. RGD-conjugated gold nanorods induce radiosensitization in melanoma cancer cells by downregulating α(v)β3 expression. Int J Nanomedicine. 2012; 7:915–24. [PubMed: 22412298]

42. Abdollahi A, Griggs DW, Zieher H, Roth A, Lipson KE, Saffrich R, et al. Inhibition of alpha(v)beta3 integrin survival signaling enhances antiangiogenic and antitumor effects of radiotherapy. Clin Cancer Res. 2005; 11:6270–79. [PubMed: 16144931]

43. Egami T, Ohuchida K, Yasui T, Mizumoto K, Onimaru M, Toma H, et al. Up-regulation of integrin beta3 in radioresistant pancreatic cancer impairs adenovirus-mediated gene therapy. Cancer Sci. 2009; 100:1902–7. [PubMed: 19604247]

44. Rieken S, Habermehl D, Mohr A, Wuerth L, Lindel K, Weber K, et al. Targeting αvβ3 and αvβ5 inhibits photon-induced hypermigration of malignant glioma cells. Radiat Oncol. 2011 doi10.1186/1748-717X-6-132.

45. Nguyen QT, Tsien RY. Fluorescence-guided surgery with live molecular navigation--a new cutting edge. Nat Rev Cancer. 2013; 13:653–62. [PubMed: 23924645]

46. Znati CA, Rosenstein M, Boucher Y, Epperly MW, Bloomer WD, Jain RK. Effect of radiation on interstitial fluid pressure and oxygenation in a human tumor xenograft. Cancer Res. 1996; 56:964–68. [PubMed: 8640786]

47. Li C, Ke S, Wu QP, Tansey W, Hunter N, Buchmiller LM, et al. Tumor irradiation enhances the tumor-specific distribution of poly(L-glutamic acid)-conjugated paclitaxel and its antitumor efficacy. Clin Cancer Res. 2000; 6:2829–34. [PubMed: 10914731]

48. Giustini AJ, Petryk AA, Hoopes PJ. Ionizing radiation increases systemic nanoparticle tumor accumulation. Nanomedicine. 2012; 8:818–21. [PubMed: 22633900]

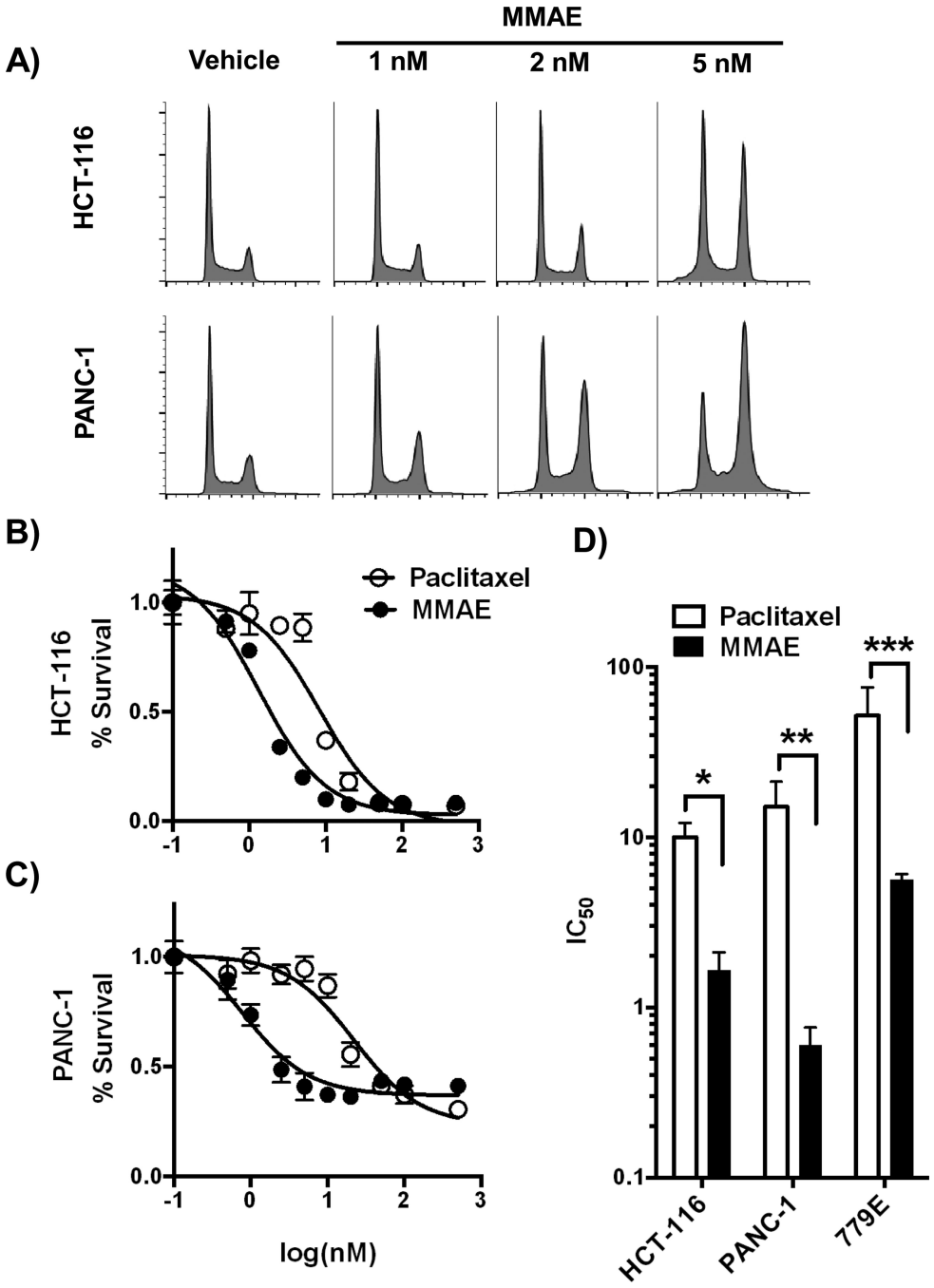


**Figure 1. MMAE has increased potency compared to paclitaxel in tumor cells**

**A)** HCT-116 (top panel) and PANC-1 (bottom panel) cells were exposed to 0, 1, 2 and 5 nM of MMAE for 24 hours. Cells were collected, stained with PI and cell cycle analyzed by FACS. **B, C)** HCT-116 and PANC-1 tumor cells were exposed to dose range of MMAE or paclitaxel for 72 hours. Cell viability was normalized to vehicle treated cells and plotted as fractional survival ± SD. **D)** $IC_{50}$ of MMAE and paclitaxel in HCT-116, PANC-1, and 779E cells. Data are plotted as mean $IC_{50}$ ± SD from triplicates. *P=0.003, **P=0.014, ***P=0.028

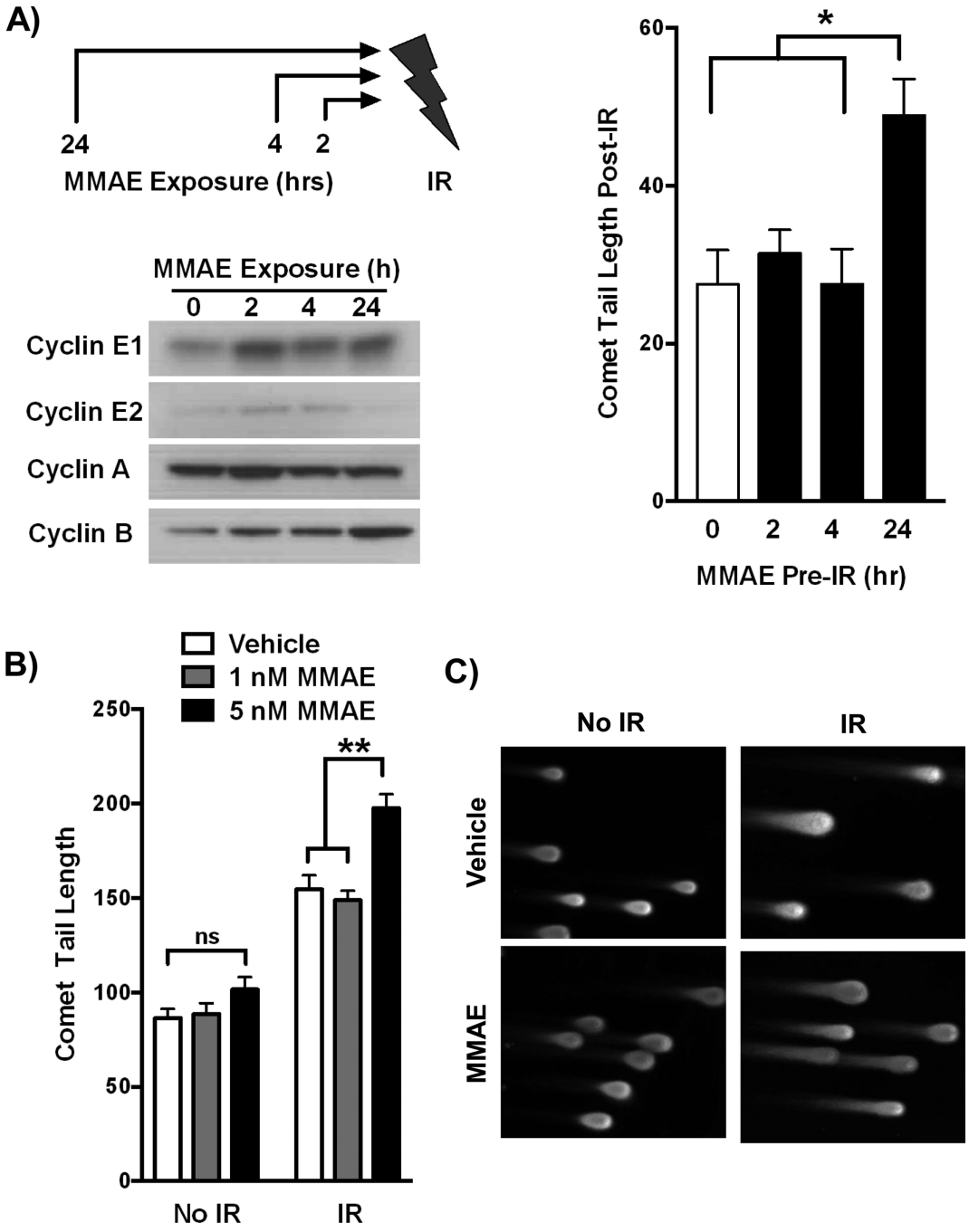


**Figure 2. MMAE increases IR induced DNA double strand breaks in a schedule and dose dependent manner**

**A)** HCT-116 cells were treated with 5 nM MMAE for 2, 4, or 24 hours followed by 6 Gy. Accumulation of cyclins was assessed by immunoblotting at time of irradiation. Comet tail length was measured using neutral comet assay 15 minutes post IR. Data are plotted as mean comet tail length ± SEM with non-irradiated comet tail length subtracted. **B, C)** HCT-116 cells were treated with 0, 1, or 5 nM MMAE for 24 hrs and then irradiated with 6 Gy. Comet tail length was measured using neutral comet assay. Data are plotted as mean comet tail

length ± SEM. Representative images from comet tail assay are shown for MMAE dose of 5 nM. *P<0.01, **P<0.0001

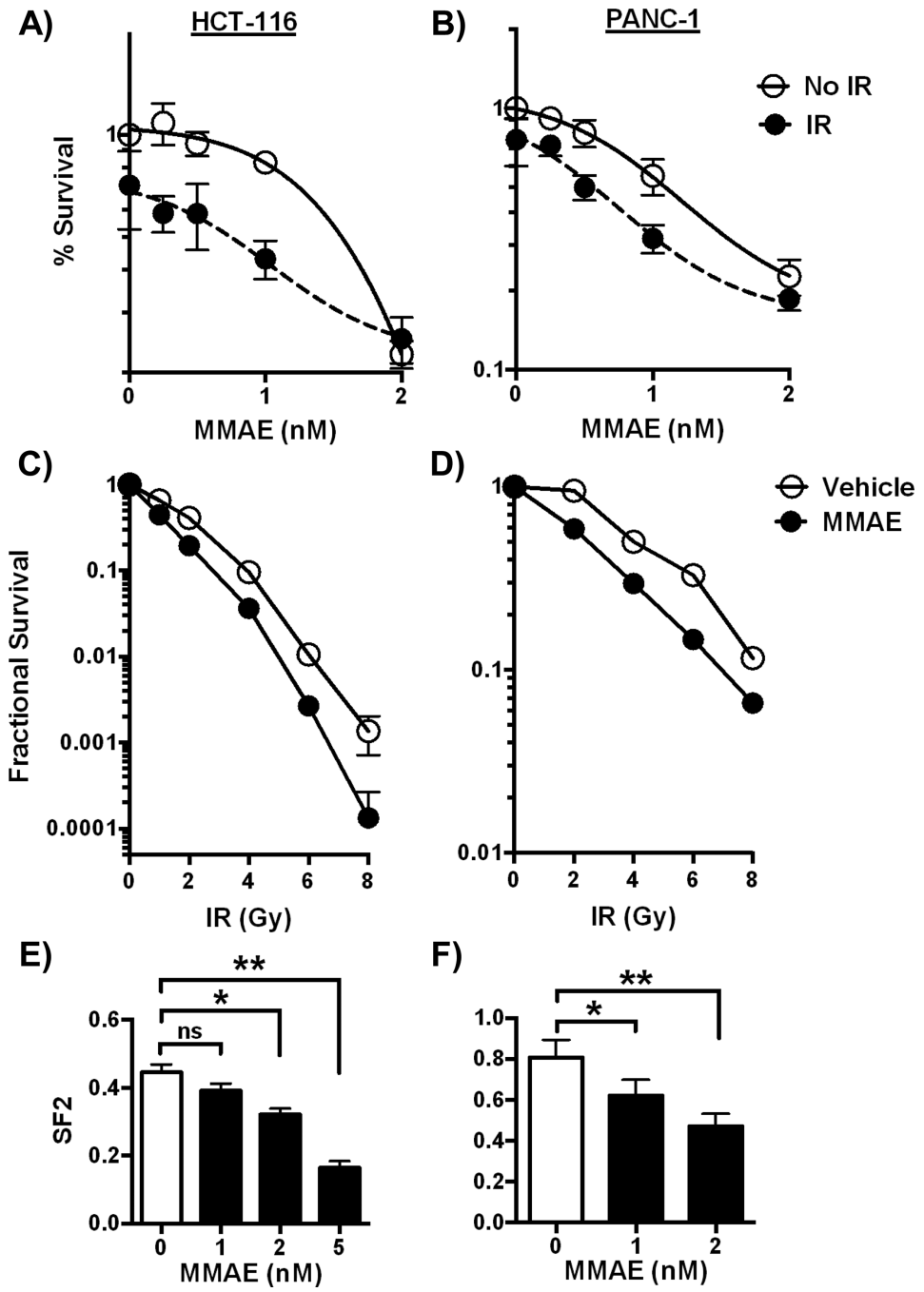


**Figure 3. MMAE decreases clonogenic survival of irradiated tumor cells**

**A, B)** HCT-116 and PANC-1 cells were exposed to varying concentrations of MMAE overnight followed by 6 Gy. Cell viability was normalized to vehicle treated, non-irradiated cells and plotted as fractional survival ± SD. **C, D)** Clonogenic survival assay to measure radiosensitization. HCT-116 and PANC-1 cells were treated with 5 and 2 nM MMAE and then irradiated. Data are plotted as mean surviving fraction ± SD. **E, F)** The effect of MMAE with 2 Gy on cell survival was measured by clonogenic survival. Survival was

normalized to non-irradiated cells for each concentration of MMAE. Data are plotted as mean survival ± SD. *P<0.01, **P<0.0001

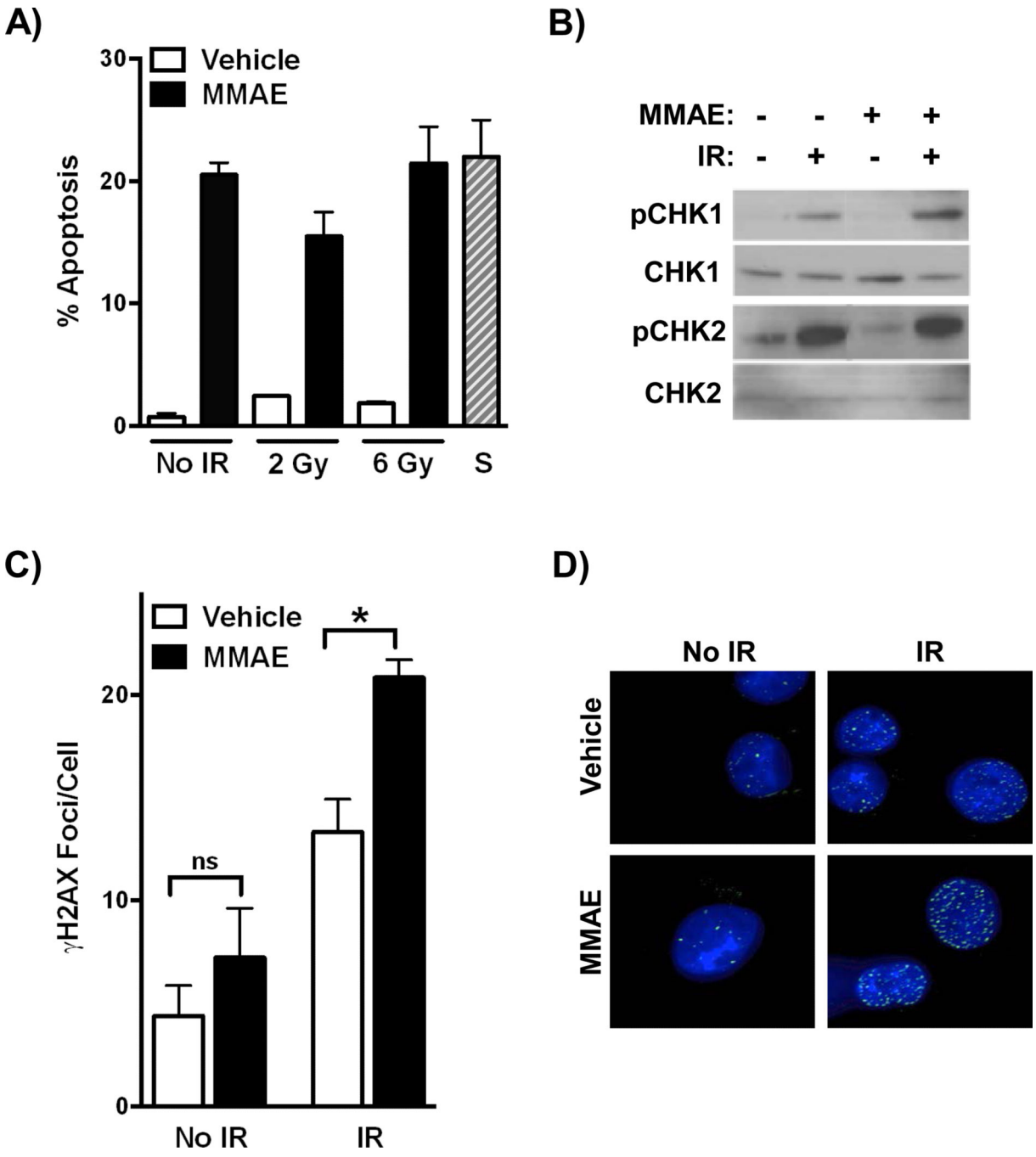


**Figure 4. MMAE increases DNA damage response in irradiated tumor cells**

**A)** HCT-116 cells were treated with MMAE for 24 hrs, irradiated and 24 hours later apoptosis measured. Staurosporine treated cells were used as a positive apoptosis control. **B, C)** HCT-116 cells were treated with MMAE for 24 hours prior to 6 Gy and were collected 2 hours later. Lysates were immunoblotted for activation of CHK1 (pS345) and CHK2 (pT68) or cells were fixed and analyzed by immunofluorescence for γH2Ax foci formation **D).** Representative images of γH2AX foci formation in PANC-1 treated cells (green). Nuclei were stained with DAPI (blue). *P<0.05

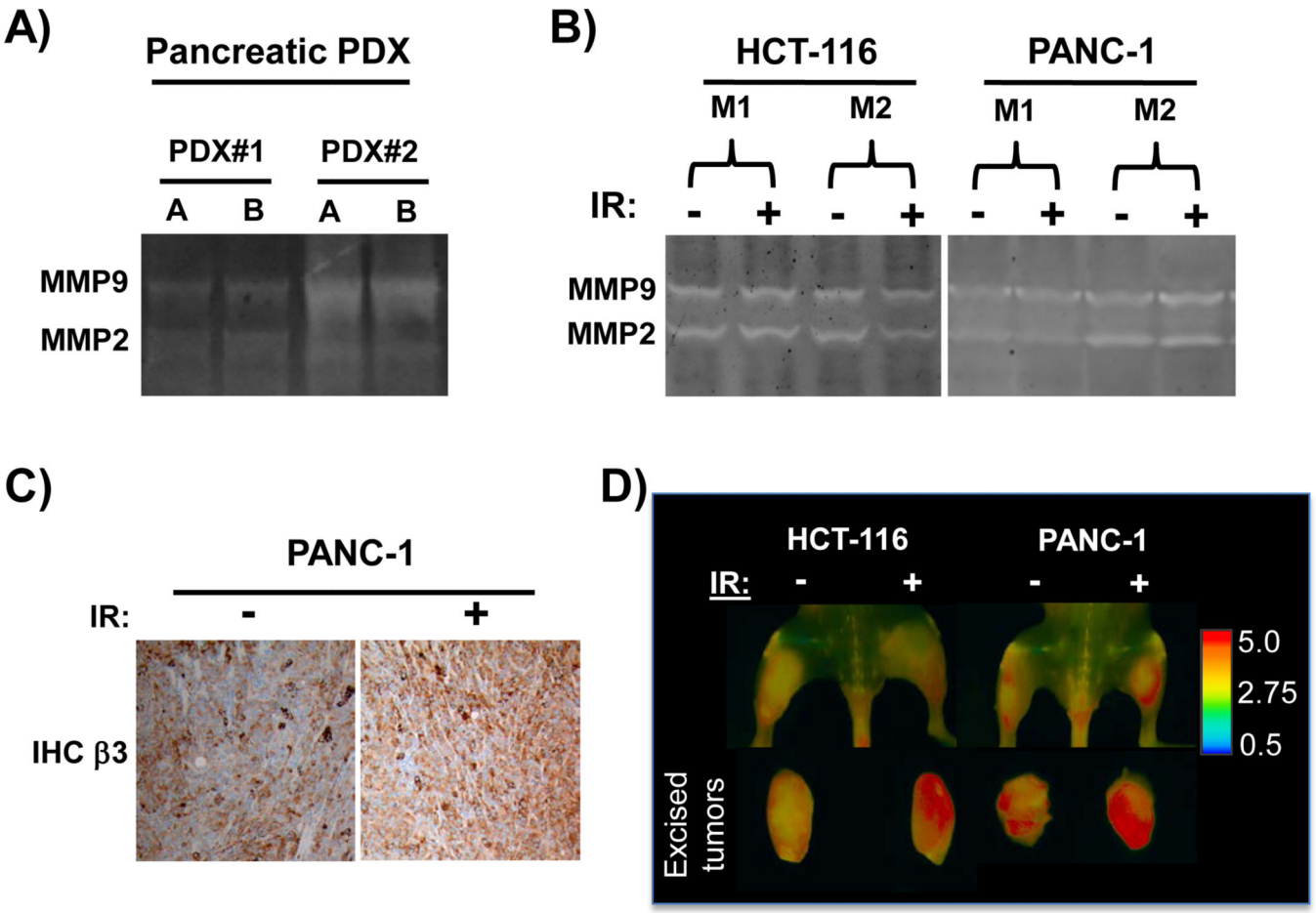


**Figure 5. Activatable cell penetrating peptides are cleaved in irradiated tumor microenvironments**

**A)** Orthotopic pancreatic adenocarcinoma PDX were harvested and zymography gels used to assess gelatinase activity, lysates. For each PDX, lysates were run in duplicate (lanes A and B). **B-D)** HCT-116 or PANC-1 tumor xenografts were grown in both the left and right hindlimbs of nude mice. The right tumor was irradiated with 6 Gy and the left tumor was shielded to block out >95% of the IR dose. **B)** Zymography gels were used to asses MMP activity in non-irradiated and irradiated tumors. **C)** β3 integrin expression by IHC in non-irradiated and irradiated PANC-1 tumors **D)** One day post IR, ratiometric ACPP was intravenously injected and Cy5:Cy7 emission ratio measured (pseudocolor scale at far right) by whole animal imaging with tumors *in situ* and after tumor excision.

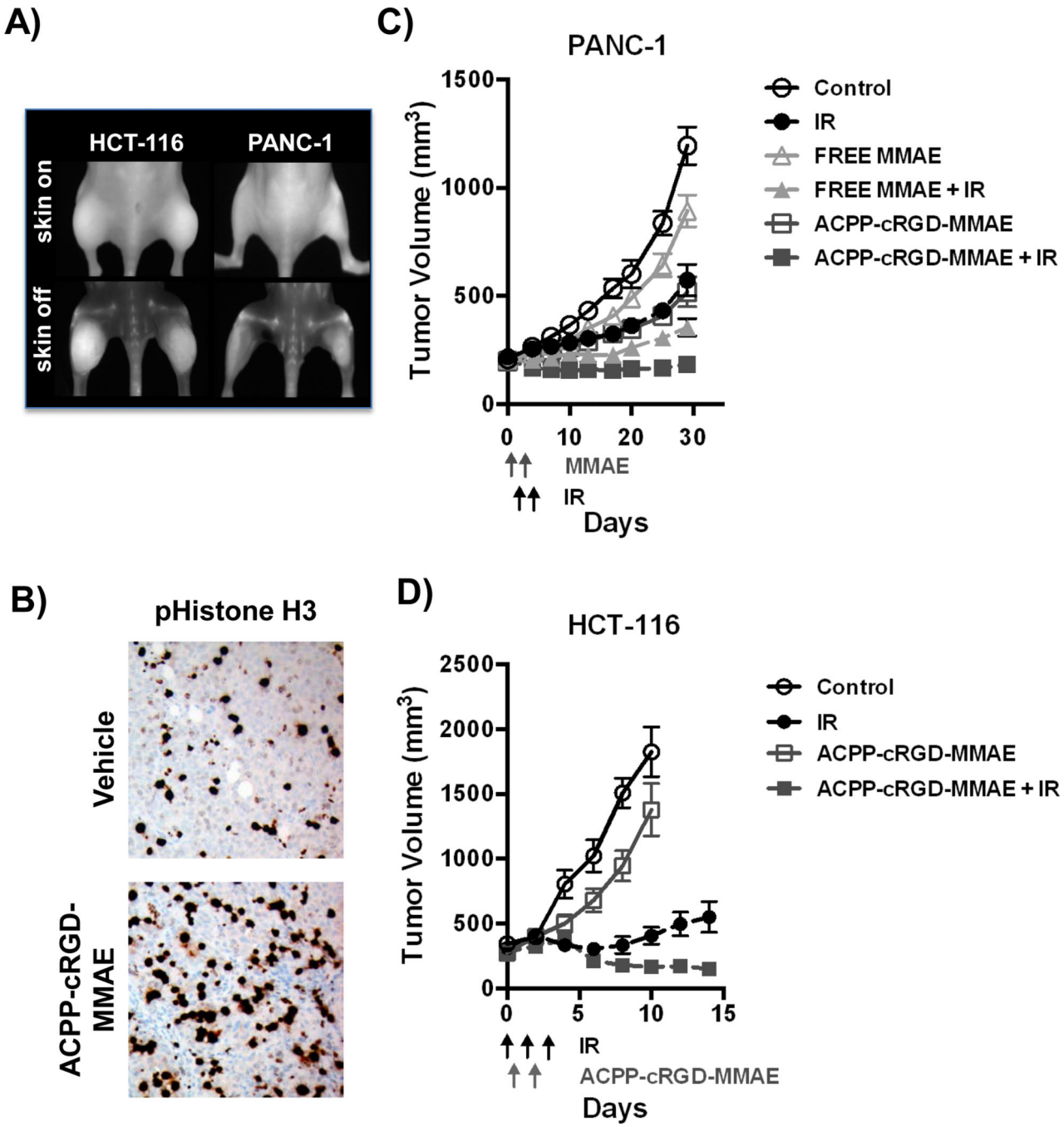


**Figure 6. ACPP-cRGD-MMAE in combination with IR significantly reduces tumor growth**

HCT-116 or PANC-1 tumor xenografts were grown subcutaneously in athymic nude mice. **A**) ACPP-cRGD-MMAE localizes to tumor xenografts following IV administration. The right hindlimb tumor was irradiated (3 Gy) while the left sided tumor was shielded to block >95% of the delivered IR dose. Cy5 labeled ACPP-cRGD-MMAE was IV injected into tumor bearing mice and mice were imaged 6 hrs later with skin on (top) and skin removed (bottom). **B)** Mice with HCT-116 tumor xenografts were IV injected with vehicle or 6 nmoles of ACPP-cRGD-MMAE. Tumor xenografts were harvested the following day,

paraffin embedded and stained for mitotic marker pS10 Histone H3. **C)** PANC-1 tumor xenografts bearing mice were IV injected with 6 nmoles of free MMAE or ACPP-cRGD-MMAE days 0 and 1. For IR treated tumor xenografts, 3 Gy was delivered on days 1 and 2. Tumors were measured twice a week. **D)** HCT-116 tumors were treated 6 Gy on day 0 and then 3 Gy on days 1 and 2. A dose of 7.5 nM ACPP-cRGD-MMAE was IV injected on both days 0 and 1, 6 hrs after IR. Tumors were measured every other day.

## Table 1

Sustained tumor growth inhibition following treatment with ACPP-cRGD-MMAE and IR.

| | V(end) / V(0) ≤ 1 | | |
|---|---|---|---|
| | **PANC-1, expt 1** | **PANC-1, expt 2** | **HCT-116** |
| **Control** | 0% | 0% | 0% |
| **IR** | 0% | 0% | 30% |
| **Free MMAE** | 0% | - | - |
| **Free MMAE + IR** | 0% | - | - |
| **ACPP-cRGD-MMAE** | 0% | 7% | 0% |
| **ACPP-cRGD-MMAE + IR** | 20% | 57% | 90% |

Percent of treated PANC-1 and HCT-116 tumor xenografts that at day 30, 40, 14 (PANC-1 (Fig 5B), PANC-1 (Supplementary Fig 5), HCT-116 (Fig 5C) respectively) post initiation of treatment were smaller than the initial tumor volume on day 0, V(end) / V(0) ≤ 1.